GaN-Based S_0-Wave Sensors on Silicon for Chemical and Biological Sensing in Liquid Environments

Xing Lu, Chi Ming Lee, Shu Yuen Wu, Ho Pui Ho, and Kei May Lau, *Fellow, IEEE*

Abstract—In this paper, we successfully developed Lamb-wave sensors in a two-port delay line topology with suspending GaN thin films on silicon substrates. The liquid insusceptibility of the lowest order symmetric mode (S_0) Lamb wave was experimentally investigated, and the relative frequency shift to water loading of the two-port S_0-wave sensors was found to be as small as 0.12%. Our GaN-on-Si sensors, exhibiting a high mass sensitivity (272 cm^2/g) and a sharp signal response at a low concentration (1 μg/mL) of anti-bovine serum albumin, were demonstrated to be suitable for chemical and biological sensing in liquid environments. In addition, the small size of the sensors and their potential to be integrated with a wide range of GaN-based devices allow for a robust, low-cost miniature sensing system to be manufactured with GaN-on-Si substrates.

Index Terms—Bio-sensor, GaN, high mass sensitivity, Lamb wave.

I. Introduction

ACOUSTIC wave sensors have been used extensively in physical, chemical, and biological analysis [1], [2]. Lamb-wave sensors differ from other acoustic wave sensors, such as quartz crystal microbalances (QCMs) and surface acoustic wave (SAW) sensors, in the configuration of the electrodes and the thickness of the medium that acoustic waves propagate in. They are typically made of a suspending, thin propagation plate ($\sim$2-μm to 7-μm thick piezoelectric membrane) with electrodes in an interlocking comb shape, also known as interdigitated transducers (IDTs) [2]–[8]. This configuration results in high mass sensitivity [2], [7], [9], strong electromechanical coupling [10], and ability to operate in liquid environments with low attenuation, making Lamb-wave sensors a competitive candidate for sensing chemical and biological substances. Recently, high performance film bulk acoustic resonator (FBAR) sensors have been demonstrated to

operate in liquid environments [11]–[13]. The two-port Lamb wave sensors in this work require a much easier fabrication process and lower overall cost, by eliminating the formation of bottom electrodes and passivation needed in FBARs.

Lamb waves, typically generated on a sufficiently thin piezoelectric membrane using IDTs, split into anti-symmetric modes and symmetric modes. Lamb-wave sensors are further classified into two types in terms of the propagation modes of Lamb-wave employed, the lowest order anti-symmetric mode (A_0), and the lowest order symmetric mode (S_0). Both modes are operational in liquids, but the signal responses of the two modes are different. The frequency shift of the A_0 wave caused by liquid loading is generally large, usually up to 18% of the unperturbed resonant frequency between unloaded state and water-loaded state [14], [15], [23], while the shift of the S_0 wave is much smaller. A_0-wave sensors are less suitable for chemical and biological sensing in a liquid environment since the shift response produced by liquid loading overwhelms the shift caused by absorption of chemical and biological substances. However, S_0-wave sensors are good candidates for chemical and biological sensing applications in liquid environments as they are sensitive to the surface mass changes resulting from chemical and biological reactions and are far less susceptible to perturbation of different liquid loadings [16]. Theoretically speaking, this is explained by the fact that the particle displacement of the S_0 wave is mainly parallel to the surface and radiation of the longitudinal component into the liquid is not significant.

Lamb-wave sensors are essentially micro mass-sensors without further modification, much like common QCMs used in e-beam metal evaporation systems to monitor depositions. Two figures of merit to evaluate cost and performance of a mass-sensor are device size and mass sensitivity. In this work, we successfully demonstrated GaN-based high-sensitivity sensors with a relatively small form factor of sensing area (0.6 mm × 2.2 mm). A small device not only has the advantage of better mechanical robustness and fabrication yield, but also of conservation of costly reagents (for chemical and biological sensing), and increased analytical throughput in diagnostic applications (as more sensing elements are encompassed in a unit area of microarrays).

The medium used to generate Lamb waves in Lamb-wave sensors is generally a sputtered polycrystalline material with piezoelectric property, mainly AlN, ZnO, and PZT [2]–[9], [17]. We believe the choice of material for fabricating Lamb-wave sensors can be extended to crystalline GaN,
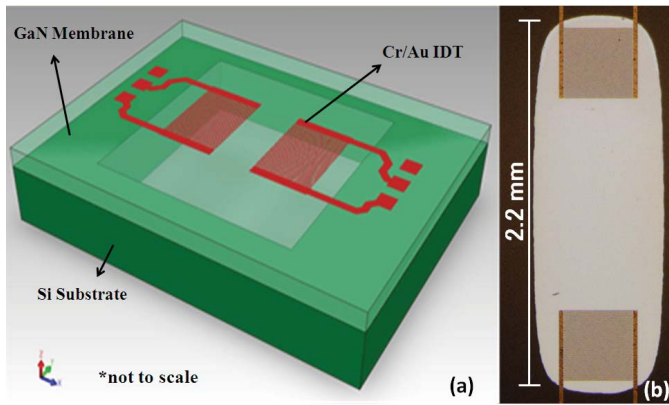
Fig. 1. (a) Schematic of the sensor structure. (b) Microphotograph of a fabricated G-II sensor (top view). Two IDTs sit on the transparent, suspending GaN membrane.

a piezoelectric material currently being exploited in the fabrication of SAW radio frequency (RF) devices [18] and FBARs [19]. Crystalline GaN, a wide bandgap (3.4 eV) semiconductor with many advantageous sensing properties, such as high acoustic velocity, and high chemical, mechanical, and thermal stability, provides an alternative choice for fabricating high-performance Lamb-wave sensors. Furthermore, GaN-based sensors can be potentially integrated with a wide range of well-developed GaN-based devices, such as high electron mobility transistors (HEMTs), light emitting diodes (LEDs), and power switches. Recently, metalorganic chemical vapor deposition (MOCVD) technology is mature enough to allow versatile sensors to be fabricated with high-quality epitaxial GaN on silicon substrates, instead of on traditional sapphire or silicon carbide (SiC) substrates, whilst conventional Si-based semiconductor processing techniques can still be adopted.

In this study, S_0-wave sensors were designed and fabricated with MOCVD-grown GaN-based thin films on silicon substrates, and further developed into a universal platform for physical and biological sensing ranged from a microbalance (mass sensor) to a specific protein-binding sensor.

II. LAMB-WAVE SENSOR DESIGN AND FABRICATION

The Lamb-wave sensors designed for this study are of two-port delay line configurations, formed by a 1-μm thick suspending GaN membrane with two Cr/Au top IDTs located near the edges of the back side cavity formed by local excavation of the silicon substrate, as shown in Fig. 1(a). Two generations of sensors (G-I and G-II) with similar configurations but different dimensions were designed in this work, and the performance of G-I sensors has been reported previously [20]. The design parameters are listed in Table I. The optical micrograph of a fabricated G-II sensor is shown in Fig. 1(b). The IDT electrodes that appear suspended in air, in fact, are mechanically supported by the transparent GaN membrane.

There are four main processing steps in the fabrication of Lamb-wave sensors, as illustrated in Fig. 2. Firstly, a stack of GaN-based epitaxial layers was grown on a high-resistivity Si (111) substrate using an Aixtron AIX-2000HT MOCVD system, as shown in Fig. 2(a). High-resistivity substrates were used to minimize electromagnetic feedthrough. The full

TABLE I
DESIGN PARAMETERS OF THE TWO TYPES OF SENSORS

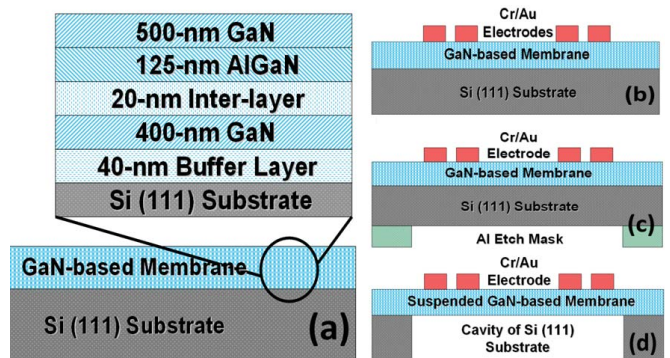| Design Parameters	G-I	G-II
IDT Period (λ)	16 μm	16 μm
Width of IDT Fingers	4 μm	4 μm
Number of Pairs in each IDT	15	20
IDT Aperture	400 μm	400 μm
Side to Side IDT Separation	240 μm (15 λ)	1440 μm (90 λ)
Thickness of the Membrane	1.085 μm	1.085 μm
Dimension of the Si Excavation	1.2 mm×1.2 mm	0.6 mm×2.2 mm

Fig. 2. Schematics illustrate the process flow of a Lamb-wave sensor. (a) Epitaxial growth of GaN-based thin film on Si substrate. Inset: Magnified diagram showing the material structure of the epi-layers. (b) Formation of the IDT electrodes on topside. (c) Patterning the etch mask on back side. (d) Release of the suspending membrane.

epitaxial stack consists of a 40-nm buffer layer and a 900-nm GaN layer. A 20-nm interlayer and a 125-nm AlGaN layer were inserted in the GaN layer to counter-balance the tensile strain produced by the mismatch of thermal expansion between the substrate and the epi-layers, and to prevent cracks on the surface. Secondly, the IDT electrodes were formed on top of the epi-layers by e-beam evaporation of Cr/Au (3 nm / 30 nm) and a liftoff process, as shown in Fig. 2(b). Thirdly, similar techniques to those in the second step were performed on the back side of the wafer to pattern a 300-nm thick Al etch mask for silicon substrate removal, as shown in Fig. 2(c). Finally, the silicon substrate was selectively removed by an SF_6-based, inductively coupled plasma (ICP) etching process for releasing the membrane. The fabrication was completed by stripping away the Al mask with a hot H_3PO_4 solution. Fig. 2(d) is a cross-sectional view of the finished device.

III. DEVICE CHARACTERIZATION

The fabricated sensors were characterized using an RF-probe station, a pair of RF-probes, and a Vector Network Analyzer. Short-Open-Load-Through (SOLT) calibration was performed prior to taking measurements, and no de-embedding was carried out. All the measurements were conducted with 50-Ω termination impedance.

A. Performance of G-I Sensors

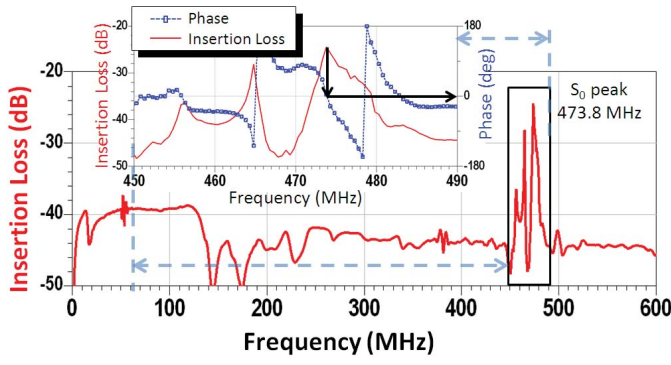The magnitude of the S_{21}-Parameter from 300 kHz to 600 MHz of an unloaded G-I sensor is shown in Fig. 3.

Fig. 3. Measured S_{21}-parameter of an unloaded G-I sensor. Inset: Magnified diagram showing the phase angle.
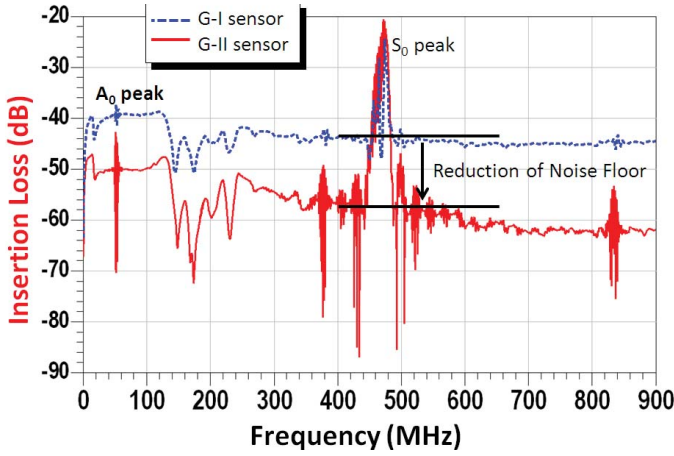

Fig. 4. Comparison of S_{21}-parameters between G-II and G-I sensors.

The peak was observed at 473.8 MHz, which indicates the propagation of the S_0 wave. The corresponding phase velocity is ∼7580m/s for the 16-μm wavelength and the 1.085-μm thick GaN-based membrane. This is in agreement with a recent publication [21]. The measured insertion loss at the resonant frequency is 24.4 dB and the noise floor near the S_0 peak is about −45 dB. The A_0 wave, appearing at around 50 MHz, is merely 2 dB above the noise floor. This suggests a weak electro-acoustic coupling and a high noise level near the A_0 peak. The A_0 wave is not included in this study.

B. Comparison Between G-II and G-I Sensors

There are three different design parameters between the two generations of sensors: the number of pairs in each IDT, the separation between two IDTs, and the dimension of the silicon excavation, as listed in Table I. Fig. 4 shows a comparison of the performance between G-II and G-I sensors.

Firstly, the signal strength of the S_0 wave in G-II sensors is –20 dB, approximately 4 dB higher than that of G-I. This can be explained by the increased number of IDT pairs (from 15 to 20), which results in a stronger electro-acoustic coupling in the G-II sensors that more than needed for compensating the attenuation induced by a longer acoustic path length.

Secondly, the noise floor around the S_0 peak is considerably lower, by more than 10 dB in G-II sensors, compared with that

of G-I. Other weak acoustic modes, such as shear horizontal acoustic plate mode (SH-APM), can also be observed in Fig. 4, but they are out of the scope of this paper. The lower noise floor in the G-II sensors is a result of the significantly increased IDT separation from 15 λ to 90 λ.

Thirdly, G-II sensors have a smaller area of silicon excavation (1.32 mm^2) than that of the G-I sensors (1.44 mm^2). This indicates that the performance improvements do not come at the expense of device size. As well, an improvement of fabrication yield and mechanical robustness in wafer handling was realized due to the reduction of suspended membrane width from 1.2 mm down to 0.6 mm.

IV. MASS SENSING EXPERIMENT

The mass sensitivities of the sensors were evaluated by loading or depositing different thicknesses of SiO$_2$ on the back side of the membranes using plasma-enhanced chemical vapor deposition (PECVD). Both the shift of resonant frequency and the phase delay, due to the mass-loading effect in the acoustic wave propagation path, were recorded by measuring the S_{21}-Parameter after each successive deposition, as previously reported in our publication [20].

The linear relationships of the frequency and the phase shift versus the thicknesses of deposited SiO$_2$ for G-I sensors are derived in Fig. 5(a) and (b), with the correlation coefficients (R^2) of 0.95834 and 0.96253, respectively. The absolute mass sensitivity in terms of frequency shift (S_{mf}) or phase shift (S_{mp}) is defined as

$$S_{mf} = \frac{\Delta f}{\Delta m} \quad \text{or} \quad S_{mp} = \frac{\Delta p}{\Delta m}$$

where Δf and Δp are the shifts of the resonant frequency and the phase produced by mass loading on the sensor surface, respectively. Δm is the loaded mass per unit area. Since

$$\Delta m = \rho \times \Delta d$$

where ρ and Δd are the density of the loaded material (2.3 g/cm^3 for PECVD SiO$_2$ [22]) and the change of thickness, respectively. Therefore

$$S_{mf} = \frac{\Delta f}{\Delta d} \cdot \frac{1}{\rho} \quad \text{or} \quad S_{mp} = \frac{\Delta p}{\Delta d} \cdot \frac{1}{\rho}$$

where $\frac{\Delta f}{\Delta d}$ and $\frac{\Delta p}{\Delta d}$ are the gradients of the linear fit in the graphs. The absolute mass sensitivities of G-I sensors in terms of frequency and phase shift are 82 GHz/(g·cm^{-2}) and 3.1×10^6 deg/(g·cm^{-2}), respectively. The normalized mass sensitivity in terms of frequency shift (sensitivity normalized by unloaded resonant frequency, 473 MHz in this case) is 174 cm^2/g.

The mass sensitivity in terms of frequency shift was compared between the two generations of sensors, as shown in Fig. 6. G-II sensors exhibit 1.6 times higher sensitivity (272 cm^2/g) and better linearity ($R^2 = 0.99812$) than G-I. This can be explained by the improved signal strength and the lower noise level in G-II sensors, as shown in Fig. 4. The larger signal to noise ratio (SNR) results in a smaller minimum distinguishable frequency shift and a more accurate measurement, i.e., a higher sensitivity.
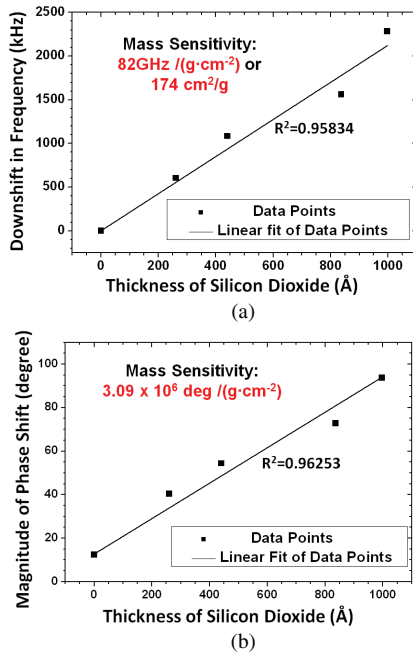
Fig. 5. Plot of (a) resonant frequency shift and (b) phase shift against the thickness of deposited SiO_2 for G-I sensors.
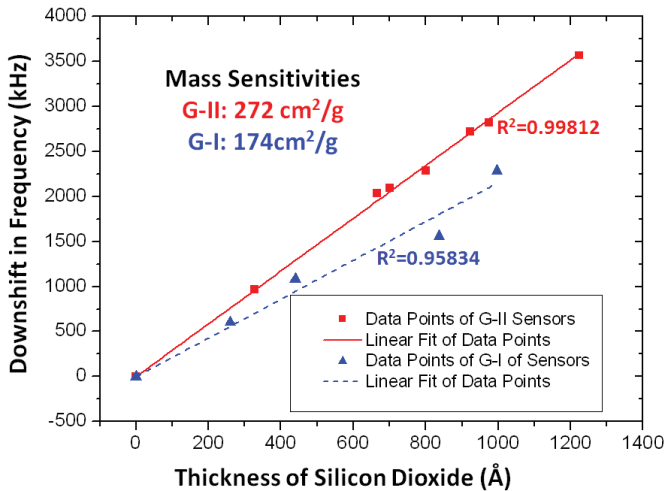

Fig. 6. Comparison of mass sensitivity between G-II and G-I sensors.

V. FLOW CELL FABRICATION AND LIQUID SUSCEPTIBILITY

This experiment was performed mainly to investigate the performance of our sensors in liquid environments, as well as the liquid susceptibility of S_0 wave, which have been less studied and understood as compared with the A_0 wave. To facilitate measurements, a flow cell system was developed for the sensors to load and unload liquid into the sensing cavity.

A. Flow Cell Fabrication

The fabrication process started with a piece of fabricated G-II sensor wafer. A 10-nm thick Au layer was sputtered on the back side of the GaN-based membrane. The Au coating not
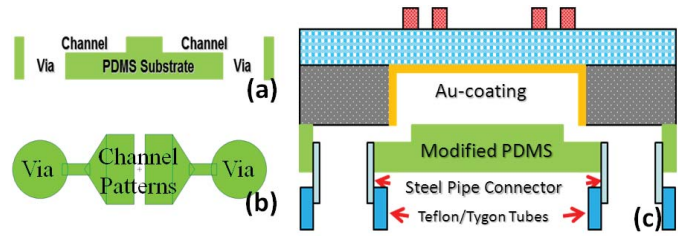

Fig. 7. (a) Cross section of the modified PDMS substrate showing the engraved flow channels and punched vias. (b) Top view of the patterns. (c) Schematic of the flow cell system.

TABLE II
SUMMARY OF THE RESULTS WHEN LOADED WITH DIFFERENT LIQUIDS

	Viscosity [mPa·s]	Density [g/cm³]	Attenuation [dB]	Freq. Shift [MHz]	Freq. Shift/ Unloaded Freq. [%]
Water	1	1	2.3	0.6	0.12
IPA	2.1	0.8	4.3	0.4	0.08

only minimized the influence caused by changes of conductivity of different liquids, but also provided an adequate surface for the protein immobilization in the subsequent biological sensing experiment. Next, the flow channels were engraved on a prepared polydimethylsiloxane (PDMS) substrate by a CO_2 laser engraving machine before vias were punched manually, as shown in Fig. 7 (a) and (b). This modified PDMS substrate was bonded onto the back side of the sensor wafer to form micro-channels. Finally, stainless steel pipe connectors were inserted into the vias of the PDMS substrate, for attaching Teflon/Tygon tubes that were connected to external liquid reservoirs, as displayed in Fig. 7 (c).

B. Liquid Susceptibility Testing

The static flow measurement was performed after the sensing cavity was filled up (observable from a microscope).

Slight frequency shift of the S_0 wave (by 0.12% of its unperturbed frequency) was observed as a result of loading with water, as illustrated in Table II. The complete switch of environments from water to Isopropenyl acetylene (IPA) caused a nuanced shift of frequency by 0.04%. The result suggests the two-port S_0-wave sensors were not susceptible to liquid loading.

A trend that attenuation increased with viscosity was also observed. Water and IPA with relative low viscosities led to a low attenuation of 2.3 dB and 4.3 dB, respectively. This suggests that the S_0-wave sensor is suitable for sensing applications in liquids with low viscosities.

The performance of the GaN-based two-port S_0-wave sensors was benchmarked with other reported results in Table III. Our sensors exhibit a comparable mass sensitivity, a relatively small size and an excellent liquid insusceptibility. Compared with the A_0-wave sensors frequency shift of up to 18%, the relative frequency shift to water loading of our S_0-wave sensors was at least 2 orders of magnitude lower. As mentioned previously, liquid insusceptibility of the S_0 wave

TABLE III
BENCHMARK OF THE STATE-OF-THE-ART LAMB-WAVE SENSORS

Spec		Operation Freq. [MHz]	Normalized Sensitivity [cm²/g]	Sensing Area [mm²]	Freq. Shift of Water Loading [%]
AlN Lamb-wave 1-port resonator (S_0) [5]		886	500	0.5	1.04
AlN Lamb-wave 2-port delay line (A_0/S_0) [23]		12/149	176/320	64	17/$_{N/A}$
ZnO Lamb-wave 2-port delay line (A_0) [24]		21	233	∼ 3	N/A
ZnO Lamb-wave 2-port delay line (A_0) [15]		18.8	207	8	18.09
This Work	G-I	473	174	1.44	N/A
	G-II	473	272	1.32	0.12

Fig. 8. Transient phase shifts during binding reaction at different concentrations.

and liquid susceptibility of the A_0 wave are attributed to the two orthogonal directions of the major oscillation components. In contrast to the one-port S_0-wave resonator sensors [25], the relative frequency shift to water loading of our two-port sensors is 1 order lower.

VI. PROTEIN SENSING EXPERIMENT

Antibodies, also known as immunoglobulins, are large Y-shaped proteins used by the immune system to identify and neutralize foreign objects in the body, such as bacteria and viruses. Early detection of certain kinds of antibody proteins in the human body may provide a warning, preventing the progress of certain diseases, such as cancers and viral infections. However, current laboratory work for detection is tedious, labor-intensive, and time-consuming. These difficulties hinder an economically viable, large-scale health care analysis for everyone. Addressing the issue, a universal biological sensing platform built on S_0-wave sensors is demonstrated, providing a viable and cost-effective solution.

In order to test the performance and versatility of our S_0-wave sensors, bovine serum albumin (BSA) was chosen. This is a protein commonly used in biological applications, such as standardizing protein concentration, and enzyme-linked immunosorbent assay (ELISA). BSA had to be immobilized on the Au-coated surface of the sensors prior to the binding reaction between antigen (BSA) and antibody (anti-BSA).
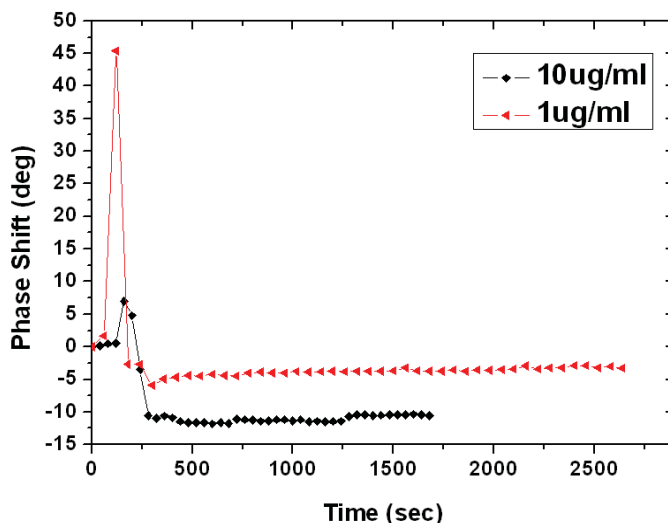
A. Modification of the Au-Coated Sensing Surface for BSA Immobilization

Firstly, 10-mM MUA (11-mercaptoundecanoic acid) in ethanol was injected into the sensing cavity and incubated for 12 hours at room temperature. The MUA formed the self-assembled monolayer (SAM) and exposed certain carboxyl groups to the Au-coated surface for further modification. Then, a 0.4-M EDC (1-Ethyl-3-[3-dimethylaminopropyl] carbodimide hydrochloride) and 0.1-M NHS (N-hydroxysuccinimide) mixture solution was injected to form activated sites on the surface for protein immobilization. Thirdly, 1-mg/ml BSA was injected and immobilized on the modified surface through the EDC/NHS activation, and the immobilized BSA acted as binding sites for anti-BSA. Finally, 1-M Ethanolamine was injected to prevent non-specific protein binding on the surface.

B. Anti-BSA Detection

After immobilizing BSA on a modified sensing surface, two different concentrations of anti-BSA solution, 10 μg/ml and 1 μg/ml, were injected into two flow cells for testing. The transient responses in phase shift of the sensors were observed using the same setup as configured previously. Fig. 8 shows the transient phase shift responses of the sensors injected with two different concentrations of anti-BSA solution. The sharp fluctuations at the beginning of the measurements indicate the noise introduced during the injections, as the thin-membrane sensors are also sensitive to the fluctuations of fluid pressure. The different fluctuations in the two curves are induced by the different fluid pressures during solution injection process.

The injections of anti-BSA solution resulted in a rapid downshift of phase angle from the pre-injected baseline, indicating the associated reaction between BSA and anti-BSA was facile. A 10-μg/ml concentration of anti-BSA caused a drift from the baseline by approximately −10 degrees, while a 1-μg/ml concentration caused a drift of approximately −4 degrees. A general trend that the phase shift responses
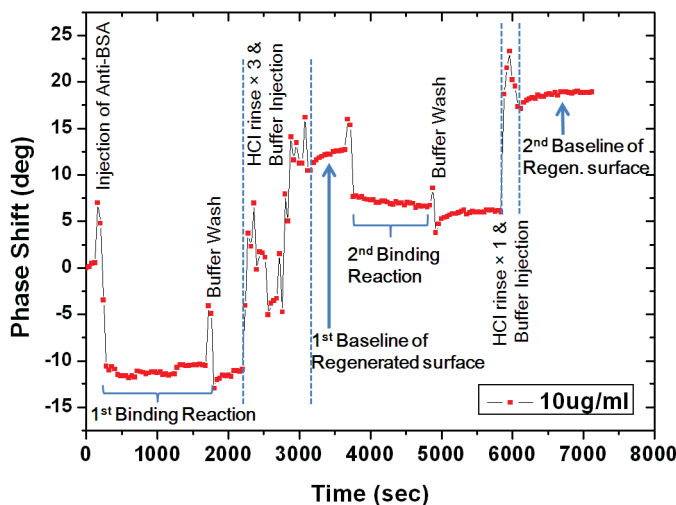
Fig. 9. Transient phase shifts of protein association and dissociation reactions.

increase with anti-BSA concentration was observed, despite their somewhat non-linear relationship.

After the BSA and anti-BSA binding reaction, dissociation reactions were performed to regenerate the sensing surface for a repeat of measurement. The transient response of the sensor injected with 10-μg/ml anti-BSA is illustrated in Fig. 9.

The first injection of anti-BSA was performed at the 200th s, and the binding reaction continued until the buffer solution (Phosphate buffered saline) wash at the 1700th s. The buffer was used to wash away the unbound anti-BSA. The phase shift produced by the first binding reaction was about –10 degrees. At the 2200th s, the regeneration process started with injecting HCl solution and rinsing 3 times, and ended with the re-injection of the buffer solution at the 3200th s. The HCl solution with a pH value of 1.5 was used to alter the shape of the bound anti-BSA which made it "unrecognizable" and dissociated from the immobilized BSA on the sensing surface. However, this regeneration process destroyed some binding sites and set free a part of the immobilized BSA, i.e., a decrease of areal mass. Therefore, it caused an unexpected upward drift of the baseline by approximately +10 degrees deviated from zero. In addition, the regenerated surface also showed a decrease of sensitivity after the second injection of anti-BSA solution at the 3700th s. The phase shift after the second binding reaction was approximately −6 degrees, less than the previous –10 degrees. This indicated a loss of binding sites. The reacted surface was again buffer-washed at the 5000th s and once again regenerated from the 5800th s to the 6000th s. This regenerated surface showed a smaller upward drift from the first regenerated baseline, approximately +5 degrees, in contrast to the previous +10 degrees. This indicated a repeat of the destruction of some binding sites and a release of some immobilized BSA on the sensing surface. The acidity of the HCl solution and the number of rinses can be fine-tuned to minimize baseline drifts.

In summary, a sensitive and reusable protein sensor based on GaN thin films on a Si substrate was demonstrated. This technology is scalable, and cost per sensor can be rapidly driven lower when production volume rises. It may provide a viable and cost-effective solution to meeting surging demand for large-scale health care analysis in the health care industry.

VII. Conclusion

Two generations of GaN-based S_0-wave sensors were successfully designed and fabricated based on a novel GaN-on-Si structure with epitaxial GaN directly grown on Si substrates. The G-II sensors delivered a comparable mass sensitivity with a relatively small formfactor of sensing area when compared with other reported results.

Experiments were conducted to develop further applications for our sensors. The S_0-wave sensors were tested and performed well in liquid environments. They were at least 2 orders of magnitude less susceptible to the perturbation of liquid mediums, as compared with the A_0-wave sensors. The liquid-loading experiment was further evolved into a protein sensing experiment. The sensors exhibited a sharp signal response to a low concentration of anti-BSA and were reusable after regeneration.

In the future, by utilizing the advanced properties of GaN S_0-wave sensors and their potential to integrate with other GaN-based devices a new sensing platform can be developed to analyze a wide range of chemical and biological reactions.

References

[1] K. Lange, B. E. Rapp, and M. Rapp, "Surface acoustic wave biosensors: A review," *Anal. Bioanal. Chem.*, vol. 391, no. 5, pp. 1509–1519, 2008.
[2] D. S. Ballantine, R. M. White, S. J. Martin, A. J. Ricco, G. C. Frye, E. T. Zellers, and E. T. Wohltjen, *Acoustic Wave Sensors: Theory, Design and Physico-Chemical Applications*. New York: Academic, 1997, p. 11.
[3] W. Y. Chang, P. H. Sung, C.H. Chu, C. J. Shih, and Y. C. Lin, "Phase detection of the two-port FPW sensor for biosensing," *IEEE Sensors J.*, vol. 8, no. 5, pp. 501–507, May 2008.
[4] S. W. Wenzel and R. M. White, "A multisensor employing an ultrasonic Lamb-wave oscillator," *IEEE Trans. Electron. Devices*, vol. 35, no. 6, pp. 735–743, Jun. 1988.
[5] R. Hino, M. Esashi, and S. Tanaka, "Antisymmetric-mode Lamb wave methanol sensor with edge reflectors for fuel cell applications," in *Proc. IEEE Int. Conf. Micro Electro Mech. Syst.*, Jan. 2010, pp. 871–874.
[6] I. Y. Huang and M. C. Lee, "Development of a FPW allergy biosensor for human IgE detection by MEMS and cystamine-based SAM technologies," *Sens. Actuators B, Chem.*, vol. 132, no. 1, pp. 340–348, 2008.
[7] R. Duhamel, L. Robert, H. Jia, F. Li, F. L. Vieudrin, J. F. Manceau, and F. Bastien, "Sensitivity of a Lamb wave sensor with 2 μm AlN membrane," in *Proc. Ultrason. SUPPL*, 2006, pp. e893–e897.
[8] J. Pepper, R. Noring, M. Klempner, B. Cunningham, A. Petrovich, R. Bousquet, C. Clapp, J. Brady, and B. Hugh, "Detection of proteins and intact microorganisms using microfabricated flexural plate silicon resonator arrays," *Sens. Actuators B, Chem.*, vol. 96, no. 3, pp. 565–575, 2003.
[9] T. Laurent, F. O. Bastien, J. C. Pommier, A. Cachard, D. Remiens, and E. Cattan, "Lamb wave and plate mode in ZnO/silicon and AlN/silicon membrane - applications to sensors able to operate in contact with liquid," *Sens. Actuators A, Phys.*, vol. 87, nos. 1–2, pp. 26–37, 2000.
[10] E. L. Adler, "Electromechanical coupling to Lamb and shear-horizontal modes in piezoelectric plates," *IEEE Trans. Ultrason., Ferroelectr., Freq. Control*, vol. 36, no. 2, pp. 223–230, Mar. 1989.
[11] H. Zhang, M. S. Marma, E. S. Kim, C. E. Mckenna, and M. E. Thmpson, "A film bulk acoustic resonator in liquid environments," *J. Micromech. Microeng.*, vol. 15, no. 10, p. 1911, Aug. 2005.

[12] G. Wingqvist, J. Bjurström, L. Liljeholm, V. Yantchev, and I. Katardjiev, "Shear mode AlN thin film electro-acoustic resonant sensor operation in viscous media," *Sens. Actuators B, Chem.*, vol. 123, no. 1, pp. 466–473, Apr. 2007.

[13] W. Xu, X. Zhang, S. Choi, and J. Chae, "A high-quality-factor film bulk acoustic resonator in liquid for biosensing applications," *J. Microelectromech. Syst.*, vol. 20, no. 1, pp. 213–220, Feb. 2011.

[14] I. A. Viketorov, *Rayleigh and Lamb Wave: Phsical Theory and Application*. Moscow, Russia: Plenum Press, 1967, p. 73.

[15] M. J. Vellekoop, *A Smart Lamb-Wave Sensor System for the Determination of Fluid Properties*. Delft, The Netherlands: Delft Univ. Press, 1994, p. 31.

[16] F. Teston, G. Feuillard, and M. Lethiecq, "Propagation of Lamb waves in 1–3 piezocomposite bordered by liquids," in *Proc. IEEE Int. Freq. Control Symp.*, vol. 2. Mar. 1999, pp. 1066–1063.

[17] Y. S. Lee, D. S. Yoon, and T. S. Kim, "Improvement of the mass sensitivity in flexural plate wave biosensor based on PZT thin film," *Integr. Ferroelectr.*, vol. 69, no. 1, pp. 391–400, 2005.

[18] T. Lalinsky, L. Rufer, G. Vanko. S. Mir, S. Hascik, Z. Mozolova, A. Vincze, and F. Uherek, "AlGaN/GaN heterostructure-based surface acoustic wave structures for chemical sensors," *Appl. Surf. Sci.*, vol. 255, no. 3, pp. 712–714, Nov. 2008.

[19] D. Neculoiu, G. Konstantinidis, A. Muller, A. Kostopoulos, D. Vasilache, K. Mutamba, C. Sydlo, H. L. Hartnagel, L. Bary, and R. Plana, "Microwave FBAR structures fabricated using micromachined GaN membranes," in *IEEE MTT-S Int. Microw. Symp. Dig.*, Jun. 2007, pp. 877–880.

[20] C. M. Lee, K. M. Wong, P. Chen, and K. M. Lau, "GaN-based Lamb-wave mass-sensors on silicon substrates," in *Proc. IEEE Sensors*, Nov. 2010, pp. 2008–2011.

[21] A. K. Pantazis, E. Gizeli, and G. Konstantinidis, "A high frequency GaN Lamb-wave sensor device," *Appl. Phys. Lett.*, vol. 96, no. 19, pp. 194103-1–194103-3, May 2010.

[22] I. Idris and O. Sugiura, "Film characteristics of low-temperature plasma-enhanced chemical vapor deposition silicon dioxide using tetraisocyanatesilane and oxygen," *Jpn. J. Appl. Phys., Regular Papers Short Notes Rev.*, vol. 37, pp. 6562–6568, Oct. 1998.

[23] F. Li, Y. Wu, J. F. Manceau, and F. Bastien, "Multi-parameter sensing in liquid using a Lamb wave based microsensor," in *Proc. Piezoelectr., Acoust. Waves, Dev. Appl., Symp.*, Dec. 2008, pp. 320–323.

[24] I. Y. Huang, M. C. Lee, and Y. W. Chang, "Development of a novel flexural plate wave biosensor for immunoglobulin-E detection by using SAM and MEMS technologies," in *Proc. IEEE Sensors*, Oct. 2006, pp. 70–73.

[25] L. Arapan, E. Anderas, I. Katardjiev, and V. Yantchev, "Sensitivity features of thin film plate acoustic wave resonators," *IEEE Sensors J.*, vol. 11, no. 12, pp. 3330–3331, Dec. 2011.

Shu Yuen Wu received the B.Sc. and M.Phil. degrees from the Department of Physics and Materials Science, City University of Hong Kong, Hong Kong, in 1998 and 2003, and the Ph.D. degree in electronic engineering from the Department of Electronic Engineering, The Chinese University of Hong Kong, Hong Kong, in 2011.

His current research interests include surface plasmon resonance sensors, biosensors, and electronic devices.

Ho Pui Ho received the B.Eng. and Ph.D. degree in electrical & electronic engineering from the University of Nottingham, Nottingham, U.K., in 1986 and 1990, respectively.

He is currently a Professor with the Department of Electronic Engineering, Chinese University of Hong Kong, Hong Kong. He has held positions as an Assistant Professor with the Department of Physics and Materials Science, City University of Hong Kong, Hong Kong from 1996 to 2002, a Senior Process Engineer with Hewlett-Packard, Bershire, U.K. from 1994 to 1996, and a Post-Doctoral with the University of Nottingham and University of Leeds from 1989 to 1994. He has published over 230 technical articles and five U.S. patents. His current research interests include nano-materials, optical instrument, and biophotonics.

Xing Lu was born in Shanxi, China, in 1986. He received the B.S. degree in microelectronics from Fudan University, Shanghai, China, in 2010. He is currently pursuing the Ph.D. degree in electronic and computer engineering with The Hong Kong University of Science and Technology (HKUST), Hong Kong.

He has been with the Photonics Technology Center and High Speed Silicon Laboratory, HKUST, since September 2010, under the supervision of Prof. K. M. Lau and Prof. C. P. Yue. His current research interests include design and implementation of the III-nitride MEMS and electronics.

Chi Ming Lee received the B.Eng. and M.Phil degrees in electronic engineering from the Hong Kong University of Science and Technology (HKUST), Hong Kong, in 2008 and 2011, respectively.

He was with the Photonics Technology Center, HKUST, from 2008 to 2011, under the supervision of Prof. K. M. Lau. His current research interests include lamb-wave sensor design, fabrication, and applications.

Kei May Lau (S'78–M'80–SM'92–F'01) received the B.S. and M.S. degrees in physics from the University of Minnesota, Minneapolis, and the Ph.D. degree in electrical engineering from Rice University, Houston, TX.

She was a Senior Engineer with M/A-COM Massachusetts, where she worked on epitaxial growth of GaAs for microwave devices, development of high-efficiency and mm-wave IMPATT diodes, and multiwafer epitaxy by the chloride transport process. She joined the Faculty of the Electrical and Computer Engineering Department, University of Massachusetts (UMass), Amherst, where she became a Professor in 1993. She initiated metalorganic chemical vapor deposition, compound semiconductor materials and devices programs at UMass. Her research group has performed studies on heterostructures, quantum wells, strained-layers, III–V selective epitaxy, high-frequency, and photonic devices. She was with MIT Lincoln Laboratory, Lexington, MA. She developed acoustic sensors with the DuPont Central Research and Development Laboratory, Wilmington, DE. She was a Visiting Professor with the Hong Kong University of Science and Technology (HKUST), Hong Kong, in 1998. She has been a Chair Professor/Professor with the Electronic and Computer Engineering Department, HKUST, since 2000. Her current research interests include III-nitride and III–V devices on silicon substrates by direct epitaxial growth.

Prof. Lau was a recipient of the National Science Foundation Faculty Awards for Women Scientists and Engineers in 1991 and Croucher Senior Research Fellowship in 2008. She served on the IEEE Electron Devices Society Administrative Committee and was an Editor of the IEEE TRANSACTIONS ON ELECTRON DEVICES from 1996 to 2002. She served on the Electronic Materials Committee, and was an Associate Editor of the Journal of Crystal Growth.